

Research on Helicopter Active Vibration Elimination Electric Actuator System Based on x-LMS Algorithm

HAO Zhenyang, YANG Jian*, ZHANG Jiawen, CAO Xin, WANG Tao

College of Automation Engineering, Nanjing University of Aeronautics and Astronautics, Nanjing 211106, P. R. China

(Received 10 May 2023; revised 20 July 2023; accepted 30 December 2023)

Abstract: When the helicopter flies forward, the aerodynamic environment will lead to the instantaneous asymmetry of aerodynamic load on the blades with different angles, which will form a large range of low-frequency vibration on the fuselage through the transmission of the infrastructure. To eliminate the vibration force with multi-directional amplitude variation, using the active control principle of structural response, an active vibration elimination electric actuator system based on the x-LMS algorithm is designed, and the vibration reduction experiment is carried out. Firstly, the scheme of two motors rotating in the same direction in a single actuator is established by comparison. Through the combination of actuators, the mathematical model of output force is deduced. Secondly, the system control block diagram of load phase difference cross-coupling is designed. For the phase outer loop with coupling, the parameter range that meets the requirements of the system stability margin is determined by the method of characteristic value of the feedback matrix, and then the optimal solution is found in the obtained parameter stability region according to the sensitivity function and input tracking performance. Then, a helicopter active vibration control system based on the x-LMS algorithm is proposed, and the damping effect of the system is verified by simulation. Finally, the experimental prototype is developed, the dynamic experiment and steady-state experiment are carried out, and the actual damping effect of the system is verified by the vibration elimination experiment.

Key words: active control of structural response; electric vibration damping actuator; characteristic value of the feedback matrix; x-LMS algorithm

CLC number: V11

Document code: A

Article ID: 1005-1120(2024)01-0053-13

0 Introduction

During the forward flight of the helicopter, a complex and asymmetric aerodynamic environment will be formed around the blades, which will cause the blades in different positions to generate unbalanced moments, resulting in serious fuselage vibration^[1]. However, excessive vibration will reduce driving comfort, affect the service life of airborne equipment, and increase the workload and cost of maintenance. Therefore, it is urgent to reduce the vibration of the helicopter^[2].

In recent years, active control of structural response (ACSR)^[3-5] has become the mainstream of helicopter vibration reduction research at home and

abroad. Ensure that the vibration level of the next generation helicopter meets the requirements specified in the US Army's directive document ADS-27 (critical components less than 0.05g)

The schematic diagram of active control of structural response is shown in Fig.1. Its basic idea is to reduce vibration in the way of "vibration cancels vibration"^[6]. The vibration information on the basic structure is collected by the sensor and sent to the vibration active controller, and the controller reverses the force and sends it to the actuator unit for execution. The actuator unit generates a force with the same frequency, amplitude, and direction as the vibration force, which is offset by the 180° diffe-

*Corresponding author, E-mail address: joy_yang@nuaa.edu.cn.

How to cite this article: HAO Zhenyang, YANG Jian, ZHANG Jiawen, et al. Research on helicopter active vibration elimination electric actuator system based on x-LMS algorithm[J]. Transactions of Nanjing University of Aeronautics and Astronautics, 2024, 41(1): 53-65.

<http://dx.doi.org/10.16356/j.1005-1120.2024.01.004>

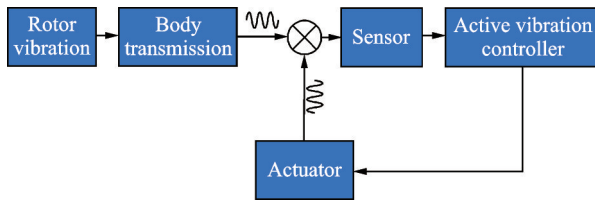


Fig.1 Schematic diagram of ACSR

rence between the phase and the vibration force to realize vibration reduction.

As the actuator of ACSR system, it plays a very key role in the whole system, so the actuator has been widely studied at home and abroad. Pusan University of Korea developed an electric vibration damper that adjusted the output force amplitude by changing the rotation radius of the eccentric mass block^[7]. Ref.[8] proposed a bilateral independent control mode algorithm with controllable output force amplitude, which was verified by a centrifugal electric damper driven by a double servo motor for eccentric load. Ref.[9] proposed a phase tracking control algorithm of adjustable mechanical active vibration damper, which can realize the online adjustment of phase. Ref.[10] described the active vibration isolation technology of ship main engine and its power device, active vibration absorption technology of power device, and active vibration elimination technology of ship structure, promoting the development of ship vibration elimination technology. Ref.[11] studied the control strategy and control algorithm of online force actuator and developed an experimental prototype, which has achieved good vibration elimination effect.

Based on the advantages of adjustable force amplitude, frequency, phase and direction, the electric vibration damping actuator system has been widely used in a new generation of non-fixed-wing aircraft vibration reduction systems^[12]. However, due to the periodic pulsating load disturbance imposed by the imbalance masses on the motor side, the stability margin of the electric actuator control system is reduced, thus increasing the difficulty of the system controller design. To solve the problem, the cross-coupling control strategy of load phase difference based on multi-input and multi-output(MIMO)^[11] is adopted. For the phase outer loop with coupling,

the parameter range meeting the requirements of system stability margin is determined by the method of characteristic value of the feedback matrix, and then the optimal solution is found in the obtained parameter stability region according to the sensitivity function and input tracking performance so that the actuator system can not only obtain the desired stability margin but also have good anti-interference performance and tracking performance.

In the active helicopter vibration damping system, the actuators are mainly installed on some non-critical nodes, and the generated actuating force is transmitted to the basic structure through the rigid body, and finally, the vibration level on the basic structure is minimized. However, because the controlled object often has variable structure, time-varying parameters, and various uncertain factors, it is difficult to optimally control the system. In order to solve the problem of the optimal weight of the output coefficients of each actuator group, this paper realizes the real-time update of the coefficient vector through the x-LMS algorithm, continuously adjusting the output of the adaptive filter^[13], and sending the generated feed forward signal to the actuator to generate actuating force. Therefore, the vibration interference of the rotor vibration on the fuselage can be accurately eliminated.

1 Model Establishment of Electric Vibration Damping Actuator

1.1 Electric vibration-damping actuator

The structure diagram of the electric vibration-damping actuator is shown in Fig.2. The imbalance mass is driven by a brushless DC motor to perform the centrifugal motion, and the required actuation force is synthesized through the centrifugal force.

There are two ways for motors in the actuator to turn in the opposite direction (reverse-rotation) and the same direction (co-rotation), as shown in Fig.3. It is specified that the rotation angular frequency of the two imbalance masses is equal, and the vertical down and horizontal left are the positive directions of the y -axis and x -axis. The output forces of two imbalance masses are obtained as

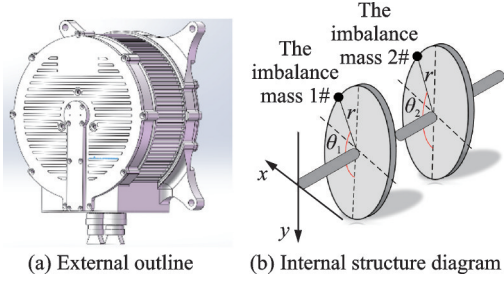


Fig.2 Structural diagram of electric vibration-damping actuators

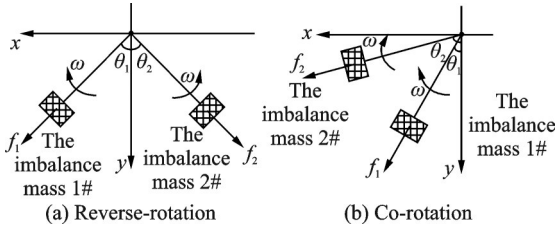


Fig.3 Imbalance masses steering diagram

$$F_1 = m\omega^2 r e^{j\theta_1}, F_2 = m\omega^2 r e^{j\theta_2} \quad (1)$$

where m is the imbalance mass, r the radius from the rotational axis to the center of each mass, and ω the rotation angular frequency of the imbalance masses. Then the synthetic force of reverse rotation F_r , and the synthetic output force of co-rotation F_i are

$$\begin{cases} F_r = 2m\omega^2 r \cos\left(\frac{\theta_1 + \theta_2}{2}\right) e^{j\frac{\theta_1 - \theta_2}{2}} \\ F_i = 2m\omega^2 r \cos\left(\frac{\theta_1 - \theta_2}{2}\right) e^{j\frac{\theta_1 + \theta_2}{2}} \end{cases} \quad (2)$$

From Eq.(2), it can be seen that the angle difference between the imbalance masses is only related to the initial phase of the masses, and the angle sum is not only related to the initial phase but also to the linear function of time. In the reverse rotation mode, the actuator can control the direction of the output force, but the amplitude is always the maximum. The co-rotation mode is just the opposite of the reverse rotation. Therefore, a single actuator cannot achieve full control of force amplitude, frequency, phase, and direction, so two actuators (A, B) are required to be used in combination, as shown in Fig.4(a).

When the reverse rotation scheme of double motors is adopted, it can be seen from Fig.4(a) that when the two actuating units coordinate control, the actuating forces with the same frequency, direction, and phase opposite actuating forces at the vibration

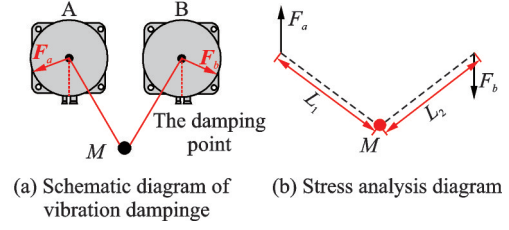


Fig.4 Vibration damping stress analysis diagram

reduction point to achieve the minimum force output. In Fig.4(b), vibration is damped at the damping point M by the combined use of the two actuators, although the output force is superimposed as 0 N, there is a torque of $M = F_a \cdot L_1 + F_b \cdot L_2$ at the damping point, and the torque changes from time to time, which makes the vibration damping unable to be carried out normally. The way of co-rotation mode is to control the amplitude of the output force first and then coordinate the control direction. When outputting the minimum force, first control $F_a = F_b = 0$, so that the synthetic torque M of the damping point is equal to 0, to effectively avoid the influence of torque in the damping process.

1.2 Establishment of mathematical model of output force

According to the above conclusion, the output force of two actuators placed in parallel is analyzed under the mode of co-rotation. Fig.5 is a schematic diagram of two actuating units arranged side by side. F_1, F_2, F_3, F_4 are the centrifugal forces acting on the mass, and F_a and F_b are the output forces of the actuating unit.

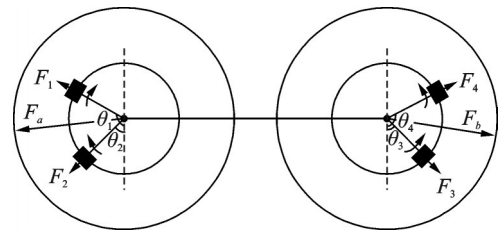


Fig.5 Schematic diagram of parallel force analysis of two working platforms

The combined force of the actuator is

$$F_a = 2m\omega^2 r \cos\left(\frac{\theta_1 - \theta_2}{2}\right) e^{j\frac{\theta_1 + \theta_2}{2}} \quad (3)$$

$$F_b = 2m\omega^2 r \cos\left(\frac{\theta_3 - \theta_4}{2}\right) e^{j\frac{\theta_3 + \theta_4}{2}} \quad (4)$$

By controlling the angle difference between the masses 1# and 2# in actuator A is equal to the angle difference between the masses 4# and 3# in actuator B, $\theta_1 - \theta_2 = \theta_4 - \theta_3$, the force amplitude is equal. The force of the multi-directional electric vibration damping actuator is obtained through the synthesis of F_a and F_b , so we have

$$F = 4m\omega^2 r \cos\left(\frac{\theta_1 - \theta_2}{2}\right) \cos\left(\frac{\theta_1 + \theta_2 + \theta_3 + \theta_4}{4}\right) e^{j\frac{\theta_1 - \theta_4}{2}} \quad (5)$$

where $\theta_1 = \omega t + \varphi_1$, $\theta_2 = \omega t + \varphi_2$, $\theta_3 = \omega t + \varphi_3$ and $\theta_4 = \omega t + \varphi_4$. φ is the phase of the output force. Assume that the output force required by the system is

$$F_{\text{out}} = F_{\text{am}} \cos(\omega^* t + \varphi) e^{j\Delta\theta^*} \quad (6)$$

where F_{am} is the amplitude of the output force.

From Eq.(5) and Eq.(6), we obtain

$$\begin{cases} \omega = \omega^* \\ \Delta\theta_1^* = \frac{\theta_1 - \theta_2}{2} = \arccos \frac{F_{\text{am}}}{4m\omega^2 r} \\ \theta^* = \frac{\theta_1 + \theta_2 + \theta_3 + \theta_4}{4} = \omega^* t + \varphi \\ \frac{\theta_1 - \theta_4}{2} = \Delta\theta_2^* \end{cases} \quad (7)$$

According to Eq.(7), the amplitude of the force is controlled by the phase difference between the two masses in single actuator ($(\theta_1 - \theta_2)/2$ or $(\theta_4 - \theta_3)/2$). The direction of the force can be controlled by the phase difference between the mass 1# and mass 4#. The phase of force is controlled by the sum phases of four masses.

2 Parameter Design and Optimization of Multi-directional Vibration Damping Electric Actuator

According to Eq.(7), the amplitude, phase and direction of force are determined by the positions of multiple masses. The traditional position loop cannot meet the precise control of force. Therefore, the position loop cross-coupling control strategy^[14] is adopted and the system block diagram is designed, as shown in Fig.6. In Fig.6, BLDC represents the brushless direct current motor, APR the automatic position regulator, ASR the automatic speed regulator, and ACR the automatic current regulator.

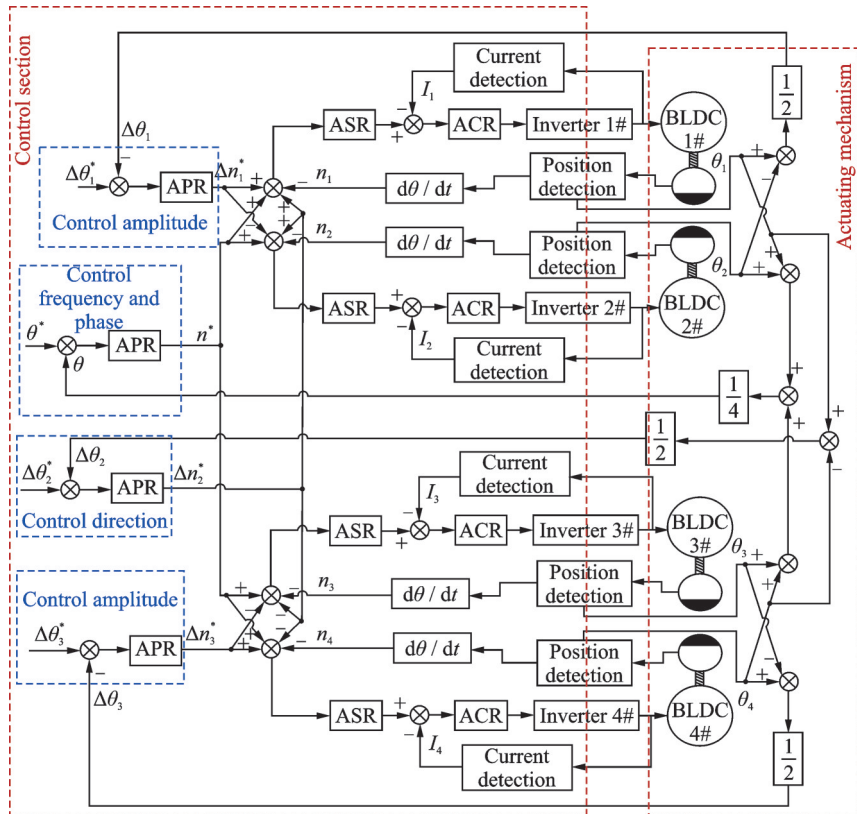


Fig.6 Control block diagram of actuator system based on load phase difference cross coupling

The control system includes two force amplitude position difference loops and one direction position difference loop. In the force amplitude loop, taking mass 1# and mass 2# as examples, the given value is $\Delta\theta_1^*$ in Eq.(7), and the feedback value is 1/2 of the actual phase difference between mass 1# and mass 2#. After making a difference, they are sent to the phase difference adjuster for calculation, and the given signal of relative speed is obtained. Because $\theta_1 - \theta_2 = \theta_4 - \theta_3$, mass 3# and mass 4# are the same. Similarly, the direction loop is given as $\Delta\theta_2^*$ in Eq.(7), and 1/2 of the difference between the output positions of mass 1# and mass 4# is taken as the feedback signal of the loop.

The setting of the phase average loop is $\theta^* = \omega^* t + \varphi$, and the feedback is the average position of the four masses. The loop has the function of adjusting the frequency of the output force and changing the phase. The relationship between the given and feedback is shown in Fig.7. The phase is changed at time t_1 , and four motors are controlled to accelerate through the position loop. The actual output force phase is given at time t_2 .

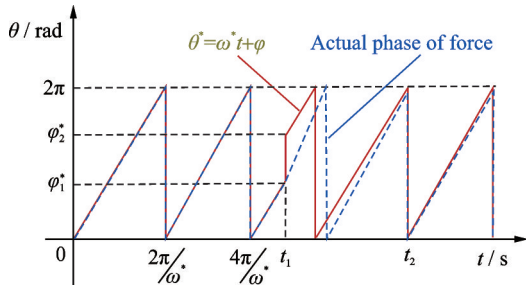


Fig.7 Input and output waveforms of output force phase regulation loop

2.1 Controller stability analysis and parameter design

2.1.1 Parameter design of inner loop of controller

For the current loop and speed loop regulators, which belong to the inner loop of the motor, the PI control can meet the loop requirements of high-frequency response. Table 1 shows the specific parameters of the driving motor used.

According to the loop parameter setting method in Ref.[15], the parameter results are shown in Table 2.

Table 1 Motor parameters

Parameter	Value
Stator winding phase resistance R_m/Ω	0.226
Stator winding phase inductance L_m/mH	0.232
Torque constant $K_T/(mN \cdot m \cdot A^{-1})$	71.2
Speed constant $K_n/(r \cdot min^{-1} \cdot V^{-1})$	134
Mechanical time constant T_m/ms	14.2
Rotor equivalent moment of inertia $J_m/(g \cdot cm^2)$	3 170

Table 2 Controller inner loop parameters

Parameter	Scale parameter	Integration parameter
Current loop	1.16	1 130.34
Speed ring	3.82	1 090.35

2.1.2 Multiple input multiple output system stability margin

For MIMO systems, based on the stability margin, the method of characteristic value of the feedback matrix is used to determine the parameter stability domain that satisfies the system phase angle margin and amplitude margin^[16]. The amplitude margin GM and phase margin PM are expressed as

$$GM = -20\lg(1 - m), PM = 2\arcsin \frac{m}{2} \quad (8)$$

In order to make the system have good dynamic and steady-state characteristics, the phase angle margin requirements should be $50^\circ \leq PM \leq 60^\circ$, and the amplitude margin requirements should be $12 \text{ dB} \leq GM \leq 20 \text{ dB}$ ^[17]. Through Eq.(8), it can be determined that the minimum eigenvalue range of the return difference matrix meeting the requirements of stability margin within the working frequency range of the system is (0.845 2, 0.9).

2.1.3 Design of position loop parameters based on hysteresis matrix method

Based on the state space method^[18], Fig.6 is converted into a simulation structure diagram of state control expression, as shown in Fig.8. In Fig.8, the input vector $\mathbf{u} = [u_1 \ u_2 \ u_3 \ u_4]^T$ corresponds to $\Delta\theta_1^*, \theta^*, \Delta\theta_2^*, \Delta\theta_3^*$ in Fig.6, and the output vector $\mathbf{y} = [y_1 \ y_2 \ y_3 \ y_4]^T$ corresponds to $\Delta\theta_1, \theta, \Delta\theta_2, \Delta\theta_3$ in Fig.6. $\mathbf{e} = [e_1 \ e_2 \ e_3 \ e_4]^T$ is the control error vector; and $\mathbf{x} = [x_1 \ x_2 \ x_3 \ x_4 \ x_5 \ x_6 \ x_7 \ x_8]^T$ the state vector, which in turn represents the speed and phase of the four eccentric mass blocks. K_{P1}, K_{P2}, K_{P3} and K_{P4} are the proportional coefficients of synchronous ring regulators. The open-loop cut-off frequency of the position loop is much smaller than the reciprocal of the

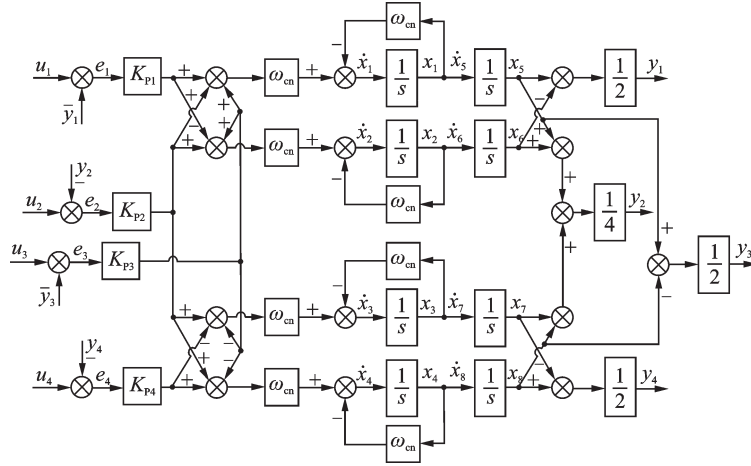


Fig.8 Control block diagram of multi-directional output force vibration-damping actuator system

time constant of each link of the speed loop. Therefore, the speed loop is simplified as a first-order inertial link. For the actuator system, it is required that its position response has no overshoot, so the four synchronizing loops are all controlled by pure proportionality.

The state-space equation of the system is established in Fig.8, shown as

$$\begin{cases} \dot{\hat{x}} = A\hat{x} + Bu \\ \mathbf{y} = C\hat{x} + Du \end{cases} \quad (9)$$

where \hat{x} is the state vector in the system, and $\dot{\hat{x}}$ the differential of the state vector. \mathbf{u} and \mathbf{y} are the input vector and output vector. A , B , C , and D are the state matrix, input matrix, output matrix, and feed-forward matrix, respectively, and their formulas are shown as

$$A = \begin{bmatrix} -\omega_{cn} I_4 & 0 \\ I_4 & 0 \end{bmatrix}_{8 \times 8}$$

$$B = \omega_{cn} \begin{bmatrix} K_{P1} & -K_{P1} & 0 & 0 & 0 & 0 & 0 & 0 \\ K_{P2} & K_{P2} & K_{P2} & K_{P2} & 0 & 0 & 0 & 0 \\ K_{P3} & K_{P3} & -K_{P3} & -K_{P3} & 0 & 0 & 0 & 0 \\ 0 & 0 & -K_{P4} & K_{P4} & 0 & 0 & 0 & 0 \end{bmatrix}^T$$

$$T(s) = I + G(s) = \begin{bmatrix} \frac{\omega_{cn} K_{P1}}{s(s + \omega_{cn})} + 1 & 0 & 0 & 0 \\ 0 & \frac{\omega_{cn} K_{P2}}{s(s + \omega_{cn})} + 1 & 0 & 0 \\ \frac{\omega_{cn} K_{P1}}{2s(s + \omega_{cn})} & 0 & \frac{\omega_{cn} K_{P3}}{s(s + \omega_{cn})} + 1 & -\frac{\omega_{cn} K_{P4}}{2s(s + \omega_{cn})} \\ 0 & 0 & 0 & \frac{\omega_{cn} K_{P4}}{s(s + \omega_{cn})} + 1 \end{bmatrix} \quad (12)$$

Assume $K_{P1} = K_{P2} = K_{P3} = K_{P4} = K_P$, the eigenvalue of $T(s)$ is

$$|\lambda| = \left| 1 + \frac{\omega_{cn} \cdot K_P}{s(s + \omega_{cn})} \right| \quad (13)$$

$$C = \begin{bmatrix} 0 & 0 & 0 & 0 & \frac{1}{2} & -\frac{1}{2} & 0 & 0 \\ 0 & 0 & 0 & 0 & \frac{1}{4} & \frac{1}{4} & \frac{1}{4} & \frac{1}{4} \\ 0 & 0 & 0 & 0 & \frac{1}{2} & 0 & 0 & -\frac{1}{2} \\ 0 & 0 & 0 & 0 & 0 & 0 & -\frac{1}{2} & \frac{1}{2} \end{bmatrix}$$

$$D = 0_{4 \times 4}$$

The system transfer function matrix is obtained

as

$$G(s) = C(sI - A)^{-1}B + D \quad (10)$$

Finally, the open-loop transfer function matrix of system is calculated as

$$G(s) = \frac{\omega_{cn}}{s(s + \omega_{cn})} \begin{bmatrix} K_{P1} & 0 & 0 & 0 \\ 0 & K_{P2} & 0 & 0 \\ \frac{K_{P1}}{2} & 0 & K_{P3} & -\frac{K_{P4}}{2} \\ 0 & 0 & 0 & K_{P4} \end{bmatrix} \quad (11)$$

Then the return difference matrix of the system

is

The premise for analyzing the stability margin of MIMO system by using the eigenvalue method of the return difference matrix is that the minimum eigenvalue of the backlash matrix is known, so let $s = j\omega$, and take the square of Eq.(13) and derivative it to zero to find the minimum value of $|\lambda(j\omega)|^2$ when Eq.(14) is satisfied

$$\omega = \sqrt{\frac{K_P \omega_{cn} + (K_P^2 \omega_{cn}^2 + 2K_P \omega_{cn}^3)^{0.5}}{2}} \quad (14)$$

$$|\lambda(j\omega)|_{\min}^2 = \frac{-2K_P \omega_{cn}}{\sqrt{K_P^2 \omega_{cn}^2 + 2K_P \omega_{cn}^3 + K_P \omega_{cn} + \omega_{cn}^2}} + 1 \quad (15)$$

It is solved that the expression of the proportion coefficient of the synchronous ring concerning the minimum eigenvalue of the return difference matrix is

$$K_P = \omega_{cn} \frac{1 - |\lambda(j\omega)|_{\min}^2}{2|\lambda(j\omega)|_{\min}^2} \left(1 + \sqrt{1 - |\lambda(j\omega)|_{\min}^2} \right) \quad (16)$$

$$0.8452 \leq |\lambda(j\omega)|_{\min} \leq 0.9 \quad (17)$$

Through Eqs.(16, 17), the value range of the proportional coefficient of the synchronous loop regulator is obtained as (134.05, 244.19).

2.2 Controller parameter optimization considering load disturbance

However, the load of the motor in the actuator system is a sinusoidal pulsating load, which leads to a large rotational speed pulsation of the imbalance mass, which affects the control accuracy of the output force. For this reason, the following will optimize the parameter stability domain based on the sensitivity H_∞ control theory to improve the anti-interference ability of the system.

The sensitivity function matrix $\mathbf{K}(s)$ of the MIMO system is the closed-loop transfer function matrix from the interference T_L to the control error $E^{[19]}$. Suppose the H_∞ norm of \mathbf{K} is defined as

$$\|\mathbf{K}\|_\infty = \sup_{\omega \in \mathbf{R}^+} \bar{\sigma}\{\mathbf{K}(j\omega)\} \quad (18)$$

According to the definition, The H_∞ norm is

the induced norm of the 2-norm of the system in H_∞ space, which reflects the maximum gain of the signal from disturbance to control error. Therefore, when the H_∞ norm of the system sensitivity function matrix $\mathbf{K}(s)$ is smaller, the influence of external disturbance on the system control error is smaller.

According to Fig.6, the control block diagram of the transfer function from the disturbance to the control error is obtained, as shown in Fig.9. In Fig.9, $T_L = [T_{L1} \ T_{L2} \ T_{L3} \ T_{L4}]^T$ is the system disturbance input vector, and $E_s = [e_1 \ e_2 \ e_3 \ e_4]^T$ the control error vector. The intermediate variable vectors are $A = [a_1 \ a_2 \ a_3 \ a_4]^T$, $B = [b_1 \ b_2 \ b_3 \ b_4]^T$, $C = [c_1 \ c_2 \ c_3 \ c_4]^T$, $D = [d_1 \ d_2 \ d_3 \ d_4]^T$, $N = [n_1 \ n_2 \ n_3 \ n_4]^T$, $\theta = [\theta_1 \ \theta_2 \ \theta_3 \ \theta_4]^T$, $Y = [y_1 \ y_2 \ y_3 \ y_4]^T$. Since the load pulsation is included in the speed loop, in order to simplify the analysis, the speed filter link and the current loop are equivalent to the first-order inertia link.

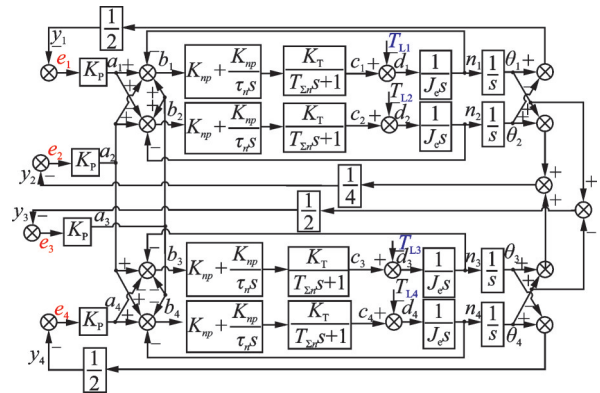


Fig.9 Block diagram of active vibration control system based on servo control strategy

The sensitivity function matrix $\mathbf{K}(s)$ of the 2-D output electric vibration-damping actuator system is

$$\mathbf{K}(s) = \begin{bmatrix} \frac{1}{2m} & -\frac{1}{2m} & 0 & 0 \\ \frac{1}{4m} & \frac{1}{4m} & \frac{1}{4m} & \frac{1}{4m} \\ \frac{m-n}{2m^2} & \frac{n}{2m^2} & -\frac{n}{2m^2} & \frac{-m+n}{2m^2} \\ 0 & 0 & -\frac{1}{2m} & \frac{1}{2m} \end{bmatrix} \quad (19)$$

$$\left\{ \begin{aligned} m &= \frac{J_e T_{\Sigma n} \tau_n s^4 + J_e \tau_n s^3 + K_{np} K_T \tau_n s^2}{(T_{\Sigma n} s + 1) \tau_n s} + \\ &\quad \frac{(K_{np} K_T + K_p K_{np} K_T \tau_n) s + K_p K_{np} K_T}{(T_{\Sigma n} s + 1) \tau_n s} \quad (20) \\ n &= \frac{K_p K_{np} K_T (1 + \tau_n s)}{2(T_{\Sigma n} s + 1) \tau_n s} \end{aligned} \right.$$

Use MATLAB to draw the maximum singular value curve of $\mathbf{K}(s)$ under different K_p , as shown in Fig.10(a). It can be seen that the H_∞ norm of the system sensitivity function $\mathbf{K}(s)$ is small, which means that the system has good dynamic performance and steady-state performance.

The step given disturbance value 1 is used to simulate the sudden change of the system load torque at 0.1 s, and the simulation waveforms under different K_p are obtained as shown in Fig.10(b). Under different K_p , the error of the synchronization loop after the system is disturbed by the load is small. However, if K_p is too large, the setting time will be longer and overshoot will occur. In order to make the system take into account the rapidity, $K_p = 150$ is finally selected. At this time, the sys-

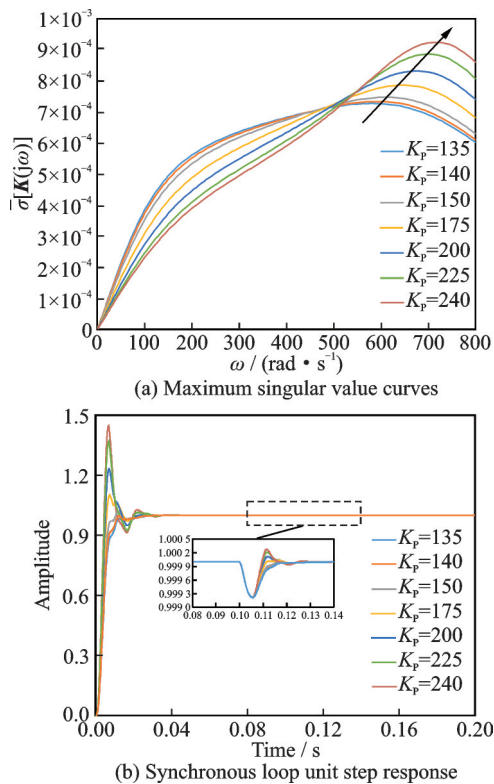


Fig.10 Maximum singular value curves and unit step response under different K_p

tem amplitude margin based on the feedback matrix eigenvalue method is 19.26 dB and the phase angle margin is 52.92° .

3 Helicopter Active Vibration Control System Based on LMS

3.1 Modeling of active vibration damping control system

Because the controlled object has variable structure, time-varying parameters, and various uncertain factors, it is difficult to establish the mathematical model of the whole vibration elimination control system, making it difficult to accurately control each actuator group in real-time. In order to solve the problem of the optimal weight of the output coefficients of each actuator group, the x-LMS algorithm proposed by Widrow and Burgess can quickly iterate in the adaptive filter to make the weight coefficients reach the optimal solution^[20].

Fig.11 shows the schematic diagram and corresponding control block diagram of the helicopter active vibration control system based on the x-LMS algorithm.

The input vector $\mathbf{X}(n)$ in Fig.11(b) represents the main rotor excitation force in Fig.11(a). $P(z)$ is the main control channel transmission from the main

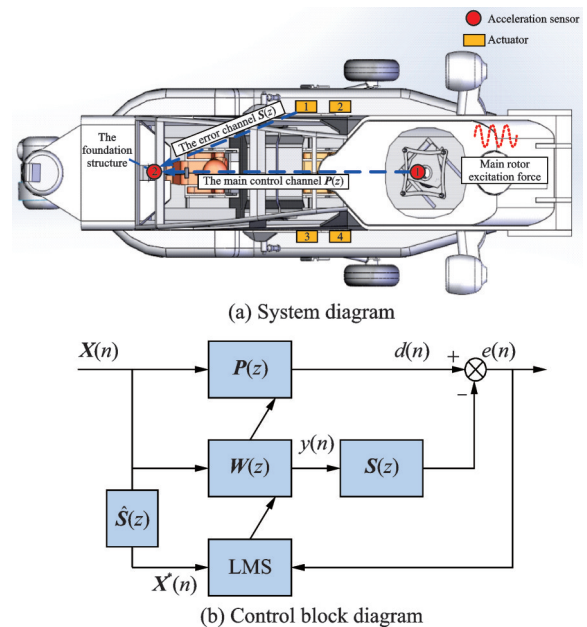


Fig.11 Helicopter active vibration control system based on x-LMS algorithm

sensor in the simulation model is 0.33, and the active vibration control system is switched in when the time is 1 s. It can be seen that the vibration force amplitude collected by the sensor decreases rapidly to around 0.026 7 and remains almost unchanged, and the vibration reduction efficiency reaches 91.75%, which meets the requirements of the system vibration reduction level.

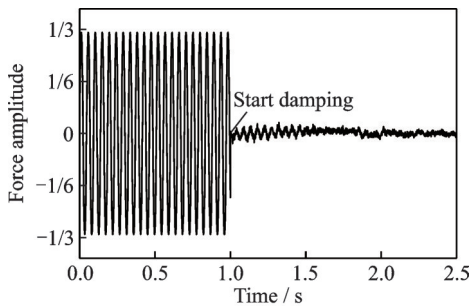


Fig.13 Vibration reduction simulation waveform of active vibration elimination control system

4 Experimental Verification of Multi-directional Vibration Damping Electric Actuator System

4.1 Experimental platform

The experimental platform of the multi-directional vibration damping electric actuator control system is shown in Fig.14, which is divided into a force measurement experimental platform and a system vibration-damping experimental platform.

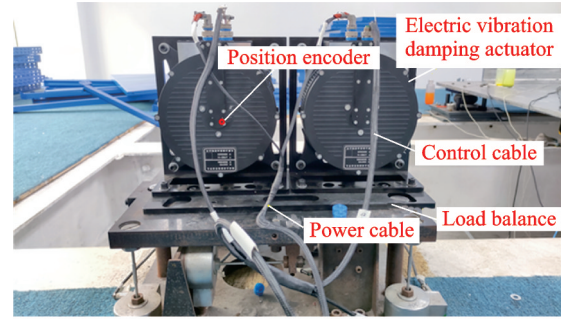
4.2 Experimental results

4.2.1 Variable force amplitude experiment

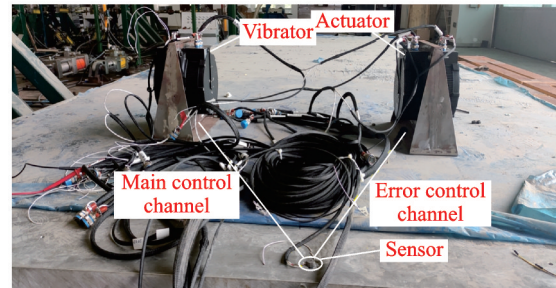
When working at 21.6 Hz, the output force amplitude is changed from the minimum force to the maximum force, every 10% of the nominal force. The experimental waveform is shown in Fig.15 and the data statistics are listed in Table 3. According to the data in Table 3, the dynamic setting time for a 10% change in the output force amplitude of the nominal force does not exceed 1 s.

4.2.2 Change direction experiment

The waveform of the output force changing



(a) Force measurement experimental platform



(b) System vibration-damping experimental platform

Fig.14 Experimental platform diagram of multi-directional vibration damping electric actuator control system

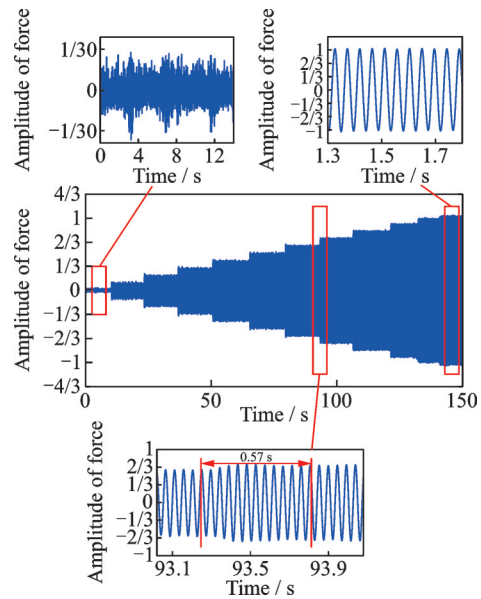


Fig.15 Experimental waveform diagram of output force amplitude change

Table 3 Dynamic variation datasheet of output force amplitude

Command	Measured value	Amplitude error/%	Response time/s
0.5	0.501	0.20	0.92
0.6	0.608	1.39	0.68
0.7	0.696	0.62	0.57
0.8	0.809	1.16	0.53
0.9	0.904	0.41	0.49
1.0	0.996	0.37	0.45

from 45° direction to horizontal direction is shown in Fig.16, where red represents the horizontal component and blue represents the vertical component. The dynamic performance is analyzed by changing the output force direction from 45° to the horizontal direction below. The dynamic setting time is 0.74 s, and the dynamic response time is less than 1 s.

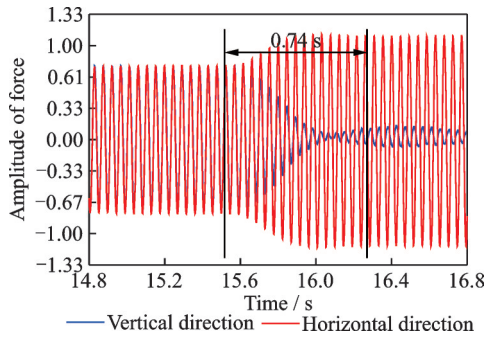


Fig.16 Experimental waveform of 45° change of output force direction

4.2.3 Phase change experiment

Experiments were conducted to change the phase of output force to 30°, 60°, 90°, and 120°, and the waveforms of 60° and 120° are shown in Fig.17.

Statistical data of phase-changing experiments are listed in Table 4. From Table 4, it can be seen that the maximum steady-state error of the output force changing phase experiment is 5.5°, and the maximum dynamic response time is 0.92 s. The dynamic and steady-state performance is good, and it can well follow the given phase value.

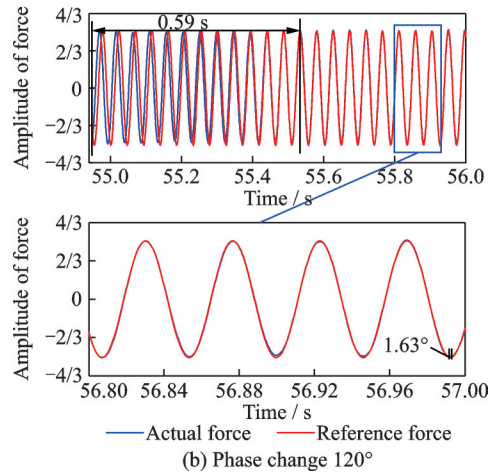
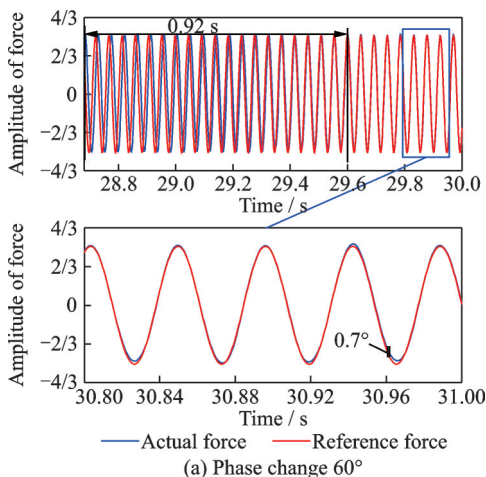


Fig.17 Phase change experiment waveform

Table 4 Dynamic variation datasheet of output force amplitude

Phase command / (°)	Phase change / (°)	Adjustment time / s	Steady-state error / (°)
30	28.80	0.61	1.40
60	63.83	0.92	0.70
90	-81.37	0.69	5.50
120	-60.00	0.59	1.63

4.2.4 Multi-directional vibration reduction experiment of the system

To verify the multi-directional vibration damping performance of the active vibration control system, the vibration force with a frequency of 21.6 Hz, a force amplitude of 0.33, and a vertical direction and a horizontal direction is generated by the vibration exciter. When the shaker reaches the rated operating point, it starts to run stably. The actuator is cut in and the acceleration data of the acceleration sensor are collected as shown in Fig.18.

Fig.18 shows the vibration damping waveforms in the vertical and horizontal directions respectively. It can be seen that the vibration level of the experimental platform is about 0.65g before the actuator system is cut in. When the actuator system is cut in, the vibration level of the experimental platform drops to around 0.05g, and the vibration-damp efficiency reaches more than 90%, which meets the requirements of the body vibration level of the fourth-generation helicopter.

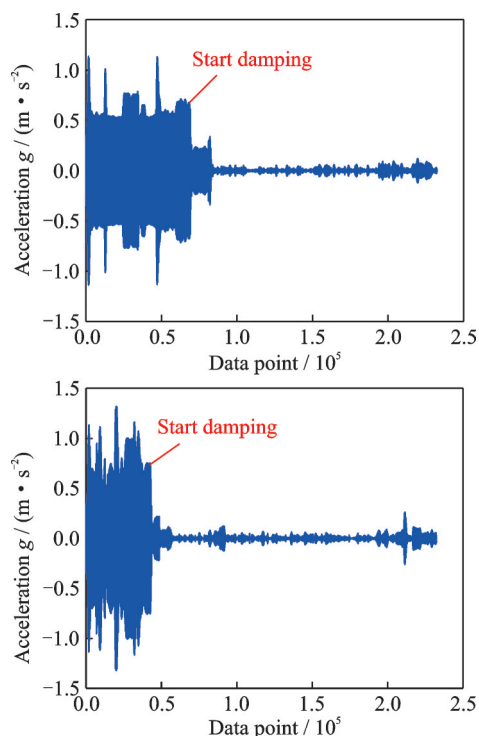


Fig.18 Waveform diagram of vibration reduction experiment of active vibration control system

5 Conclusions

Aiming at the vibration problem of helicoptering, an active vibration damping electric actuator system based on the LMS algorithm is proposed in this paper. The following conclusions are obtained:

(1) By comparing the torques of two motors in a single actuator in the same direction and the opposite direction, the scheme of the same direction rotation was established. The mathematical model of multi-direction output force is derived by placing actuators in parallel. It can meet the functional requirements of variable amplitude, frequency, phase, and direction of output force.

(2) For the synchronization loop with a cross-coupling effect, the feedback matrix eigenvalue method of the MIMO system is used to determine the parameter stability range that meets the requirements of amplitude margin and phase angle margin, and then based on the sensitivity function and input tracking performance, the optimization is carried out in the parameter stability domain, and finally, determine the parameters that make the system take into account both good dynamic and steady performance and anti-interference.

(3) A helicopter active vibration damping con-

trol system based on LMS is designed, the system is modeled and the vibration reduction effect of the system is verified by MATLAB simulation.

(4) The designed parameters are used to measure force and eliminate vibration of the multi-direction output force electric vibration damping system, and the damping effect of the system, as well as the response and robustness of the parameters, are verified.

References

- [1] ZHU Hongyan, WU Baochang, WANG Gang, et al. Research progress of helicopter vibration active control technology[C]//Proceedings of 2020 China Aviation Industry Technology and Equipment Engineering Association Annual Conference. [S.l.]:[s.n.], 2020. (in Chinese)
- [2] LIU Guoqiang, DONG Mingming, QIN Hao. Effects of helicopter vibration and noise combined environment on human body[J]. Aviation Science and Technology, 2016,27(11): 30-33. (in Chinese)
- [3] MILLOTT T A, ROBERT G K, JONATHAN K, et al. Risk reduction flight test of a pre-production active vibration control system for the UH-60M[C]//Proceedings of American Helicopter Society 59th Annual Forum. Phoenix,USA: AHS, 2003.
- [4] ROBERT G K, MILLOTT T A. Development and flight testing of the active vibration control system for the Sikorsky S-92[C]//Proceedings of American Helicopter Society 56th Annual Forum. Virginia, USA: AHS,2000.
- [5] VIGNAL B, KRYSINSKI T. Development and qualification of active vibration control system for the Eurocopter EC225 / EC725[C]//Proceedings of American Helicopter Society 61st Annual Forum. Grapevine,USA: AHS, 2005.
- [6] KING S P. Minimisation of helicopter vibration through active control of structural response[M]//Rotorcraft Design for Operations. [S.l.]: AGARD, 1987.
- [7] HAN Guangcai, LI Hong, WANG Zhiqiu. Research on ship electric vibration damping actuator[J]. Journal of Harbin Engineering University, 2005(1): 39-43. (in Chinese)
- [8] KENNETH D G. Modular vibratory force generator, and method of operating same: United States, 5903077[P]. 1999-05-11.
- [9] LU Xiqun, WANG Dongjun, ZHANG Aidong. Experimental research on active vibration control based on mechanical actuator[J]. Noise and Vibration Control, 2008(4): 1-2, 5. (in Chinese)
- [10] YANG Tiejun, JIN Guoyong, LI Wanyou, et al. Research on active vibration control technology of ship

- power plant[J]. Ship Science and Technology, 2006 (S2): 46-53.
- [11] HAO Zhenyang, WANG Tao, CAO Xin, et al. Position loop decoupling control strategy for anti-vibration electric actuator[J]. Acta Aeronautica et Astronautica Sinica, 2022, 43(8): 605-620.
- [12] YOU Xiaoliang. Research on the key technology of centrifugal actuator for active vibration control[D]. Nanjing: Nanjing University of Aeronautics and Astronautics, 2013. (in Chinese)
- [13] MUKHOPADHYAY V, NEWSOM J. Application of matrix singular value properties for evaluating gain and phase margin of multiloop systems[C]//Proceedings of AIAA Guidance Navigation and Control Conference. San Diego, CA: AIAA, 1982.
- [14] HAO Zhenyang, LI Xue, CAO Xin, et al. A cross-coupled control strategy of phase difference for electric vibration damping actuator[J]. IEEE Access, 2021 (9): 10988-11001.
- [15] TENG Fulin. Research and practice of permanent magnet synchronous motor servo system control strategy[D]. Nanjing: Nanjing University of Aeronautics and Astronautics, 2009. (in Chinese)
- [16] LI Xindong, GOU Xingyu. Analysis and improvement of stability margin of multiple input multiple output linear steady system[J]. Control Theory and Application, 2014, 31(1): 105-111. (in Chinese)
- [17] HU Shousong. The principle of automatic control[M]. 5th ed. Beijing: Science Press, 2007: 214-217. (in Chinese)
- [18] ZHU Xiyan. Direct solution of state equation from system block diagram[J]. Computer Simulation, 1990 (4): 14-18. (in Chinese)
- [19] ZHAI Fucun, SHI Zhongke, DAI Guanzhong. Several definitions of stability margin of MIMO system[J]. Flight Mechanics, 2002, 20(2): 6-9. (in Chinese)
- [20] WIDROW B, STERN S D. Adaptive signal processing[M]. Englewood Cliffs, NJ: Prentice Hall, 1985.
- Acknowledgements** This work was supported by the National Natural Science Foundation of China (No. 52077100) and the Aviation Science Foundation (No. 201958052001).
- Author** Prof. HAO Zhenyang received the B.S. degree in electrical engineering from Nanjing Normal University, in 2004, and the M.S. and Ph.D. degrees in power electronics and motion drive from the Nanjing University of Aeronautics and Astronautics, in 2007 and 2010. He has been an professor in the Department of Electrical Engineering, Nanjing University of Aeronautics and Astronautics, since 2021. His current research interests include servo control of permanent magnet synchronous, motorsensorless control technology and new energy power electronic conversion technology.
- Mr. YANG Jian received his M.S. degree in electrical engineering from the College of Automation Engineering, Nanjing University of Aeronautics and Astronautics, majoring in motor control.
- Author contributions** Prof. HAO Zhenyang proposed the subject and designed the subject framework. Mr. YANG Jian designed the simulation model, conducted the experimental verification and wrote the manuscript. Mr. ZHANG Jiawen designed system parameters and assisted in experiments. Prof. CAO Xin revised and modified the manuscript. Mr. WANG Tao summarized and sorted out the experimental results. All authors commented on the manuscript draft and approved the submission
- Competing interests** The authors declare no competing interests.

(Production Editor: SUN Jing)

基于 x-LMS 算法的直升机主动消振电力作动器系统研究

郝振洋, 杨 健, 张嘉文, 曹 鑫, 王 涛

(南京航空航天大学自动化学院, 南京 211106, 中国)

摘要: 直升机前飞时, 气动环境会导致不同方位角的桨叶出现气动载荷的瞬间不对称, 通过基础结构传递会在机身形成大幅度的低频振动。为了消除多方向幅值变化的振动力, 利用结构响应主动控制原理, 设计了基于 x-LMS 算法的主动消振电力作动器系统, 并进行了减振实验。首先, 通过比较确定了单台作动器中两台电机同向旋转的方案。通过两台作动器的组合使用, 推导出输出力的数学模型。其次, 采用负载相位差交叉耦合的控制策略设计系统控制框图。针对存在耦合的相位外环, 通过回差阵特征值法确定满足系统稳定裕度要求的参数范围, 再根据灵敏度函数和输入跟踪性能在所得的参数稳定域内寻找最优解。然后, 提出了基于 x-LMS 算法的直升机主动振动控制系统, 并通过仿真实验验证了该系统的减振效果。最后, 研制的实验样机进行了动稳态实验以及减振实验, 验证了系统的实际减振效果。

关键词: 结构响应主动控制; 消振电力作动器; 回差阵特征值法; x-LMS 算法